



A global analysis of the high- P_T dilepton sample using 360 pb^{-1} of Run 2 data

Sebastian Carron, Doug Benjamin, Mircea Coca, Mark Kruse
Duke University
(for the CDF collaboration)

Abstract

We present results from a new technique of globally fitting the high- P_T dilepton sample. One advantage of this analysis is that no events are lost from event cuts after the requirement of 2 high- P_T leptons (with a caveat for the ee and $\mu\mu$ channels as will become clear), and the separation of the main processes that constitute this sample in a \cancel{E}_T - N_{jet} phase space allows one to fit for each standard model (SM) contribution. Additionally, in the future this analysis can be extended into a general search for physics beyond the standard model in the dilepton channel.

Here we present our measurements of the $t\bar{t}$, WW and $Z \rightarrow \tau\tau$ cross sections with 360 pb^{-1} of data. The results from the analysis are:

$\sigma(t\bar{t}) = 8.4_{-2.1}^{+2.5}(\text{fit})_{-0.3}^{+0.7}(\text{shape})$, and $\sigma(WW) = 16.1_{-4.3}^{+5.0}(\text{fit})_{-0.2}^{+0.8}(\text{shape})$ pb extracted using all dilepton channels ($ee + \mu\mu + e\mu$), and $\sigma(Z/\gamma^* \rightarrow \tau\tau) = 292.7_{-45.1}^{+48.9}(\text{fit})_{-2.9}^{+5.9}(\text{shape})$ pb from the $e\mu$ channel only. This approach has potential to provide significant statistical gain over more traditional measurements. Looser selection criteria and other applications of this method are being explored..

Contents

1	Motivation and Methodology	3
2	Lepton ID and Event Selection	3
3	Signal acceptances	4
4	Background acceptances	5
5	Data and grand summary of expectations	5
6	The \cancel{E}_T-N_{jet} distributions for data and MC	6
7	The Likelihood fit technique	8
8	$Z \rightarrow \tau\tau$ cross-section additional considerations.	9
9	Systematics	10
9.1	Acceptance systematics	10
9.2	Shape systematics	10
10	Fit results	11
11	Conclusions	13
12	Acknowledgments	13

1 Motivation and Methodology

This analysis was developed as a more global means of understanding the content of the high- P_T dilepton sample. After the requirement of 2 high- P_T leptons only, we consider the processes that can make up this sample and ask the question what other objects can exist in these events. The answer is neutrinos (which give \cancel{E}_T) and jets (either from decays of final state objects, or from initial or final state radiation). So the most straightforward thing to do is simply fit the \cancel{E}_T vs. N_{jet} 2-D distribution from the data to those from the expected SM contributions, to extract the cross-sections from these contributions. As will be shown, this works because of a very nice (fortuitous?) feature of this sample: the main contributions appear in very different regions of the \cancel{E}_T vs. N_{jet} phase space because of their different sources of \cancel{E}_T and jets.

Our current analysis extracts $t\bar{t}$, WW , and the $Z \rightarrow \tau\tau$ cross-sections in an independent and more inclusive way to the counting experiment analysis.

The main processes that contribute to the $e\mu$ channel are WW , $Z \rightarrow \tau\tau$ and $t\bar{t}$, and it is for these processes we want to extract cross-sections. Additionally we have a fake lepton contribution in $W + jet$ and $W\gamma$ events, and also WZ and ZZ contributions. In the ee and $\mu\mu$ channels we also have a large $Z/\gamma^* \rightarrow ee$ and $Z/\gamma^* \rightarrow \mu\mu$ Drell-Yan contribution, which we significantly reduce by making a \cancel{E}_T significance cut (briefly described later). These latter smaller contributions we fix in all our fits, normalized to their expected values for a given integrated luminosity.

We fit the cross sections of our main signals: WW $Z \rightarrow \tau\tau$ and $t\bar{t}$ in the $e\mu$ channel fit. In the specific cases of the ee and $\mu\mu$ channels, we only fit the WW and $t\bar{t}$ cross sections, since the additional cut we apply in these channels makes it hard to extract the $Z \rightarrow \tau\tau$ cross section.

Besides electrons and muons in all of these sources, the only other objects are jets and neutrinos. We maximally exploit this fact by not cutting on variables related to these objects, but rather fitting the data in the 2-D \cancel{E}_T - N_{jet} phase space to the expected sources. The strength of this approach lies in the very different regions of \cancel{E}_T - N_{jet} space occupied by the relatively few SM processes contributing to the high- P_T dilepton sample.

2 Lepton ID and Event Selection

The sample we fit consists of two oppositely charged leptons (electrons or muons) isolated from other activity in the event. Table 1 lists the requirements we make on the sample that we then fit in the \cancel{E}_T - N_{jet} phase space.

Lepton ID
Track and Calorimeter Isolation on the leptons
Conversion and Cosmic-Ray filter
If ee or $\mu\mu$: $\cancel{E}_T^{sig} > 2.5\sqrt{GeV}$
Opposite sign leptons

Table 1: Requirements for the Dilepton sample used in the Inclusive Dilepton Analysis.

Because Drell-Yan events have no real missing transverse energy, \cancel{E}_T (no neutrinos), a cut on \cancel{E}_T significance in the ee and $\mu\mu$ channels is very effective in reducing this background while preserving most of the signals with real \cancel{E}_T (it does however significantly reduce $Z \rightarrow \tau\tau$ also which means we only fit for this signal in the $e\mu$ channel). \cancel{E}_T significance is defined by:

$$\cancel{E}_T^{sig} = \frac{\cancel{E}_T}{\sqrt{\sum E_T}}$$

where $\sum E_T$ is over all (raw) calorimeter towers, and is corrected to take into account the P_T of the muons. We cut at a value of $2.5 \sqrt{\text{GeV}}$.

We use both central and forward electrons from our detector. Central electrons deposit all their energy in the central electromagnetic calorimeter and are matched to a track from the Central Outer Tracker (COT). Forward electrons are detected in the forward electromagnetic calorimeter and are matched to tracks from the silicon detector. Muons are required to be minimum ionizing in the electromagnetic and hadronic calorimeters and to be matched to tracks in the muon detectors when pointing to those detectors..

In addition to leptons, the processes we are studying can have neutrinos which manifest themselves as missing energy (\cancel{E}_T), and partons which manifest themselves as jets. As mentioned it is precisely these two quantities that we fit the dilepton data to. We apply all standard CDF corrections to both the \cancel{E}_T and jet energies.

3 Signal acceptances

A summary of the samples used for $t\bar{t}$, WW , and $Z \rightarrow \tau\tau$ is given in Table 2. We used Herwig for the WW signal, Pythia for $t\bar{t}$ and Pythia with TAUOLA decaying the τ 's for the $Z \rightarrow \tau\tau$ signal. Table 3 summarizes the acceptances by dilepton categories for the three signal processes. The acceptances shown are *after* applying trigger and lepton ID scale factors, as well as other corrections.

	Generator	Number of Events	Assumed σ (pb)	Luminosity (fb^{-1})
$t\bar{t}$	PYTHIA	1142339	6.1	187 fb^{-1}
WW	PYTHIA	3295522 (leptonic forced decays)	12.5	2568 fb^{-1}
$Z \rightarrow \tau\tau$	PYTHIA	2525739	337.5	7.5 fb^{-1}

Table 2: Summary of MC samples used for $t\bar{t}$, WW and $Z \rightarrow \tau\tau$, and the effective total luminosity of these samples.

	$e\mu$	ee	$\mu\mu$	$\ell\ell$
$t\bar{t}$	$(0.40 \pm 0.006)\%$ 10.0 ± 0.7	$(0.14 \pm 0.003)\%$ 3.6 ± 0.5	$(0.14 \pm 0.003)\%$ 3.4 ± 0.4	$(0.68 \pm 0.013)\%$ 17 ± 1.6
WW	$(0.30 \pm 0.001)\%$ 13.8 ± 0.8	$(0.11 \pm 0.0006)\%$ 5.2 ± 0.4	$(0.09 \pm 0.0005)\%$ 4.3 ± 0.3	$(0.50 \pm 0.002)\%$ 23.3 ± 1.5
$Z \rightarrow \tau\tau$	$(0.046 \pm 0.0005)\%$ 57.8 ± 4	$(0.0008 \pm 0.00007)\%$ 1.1 ± 0.2	$(0.0005 \pm 0.00005)\%$ 0.6 ± 0.1	$(0.047 \pm 0.0006)\%$ 59.9 ± 4.3

Table 3: Summary of acceptances (first row) and expected numbers of events, for $t\bar{t}$, WW , and $Z \rightarrow \tau\tau$. These are corrected for the scale factors mentioned in the text. Errors are statistical only.

4 Background acceptances

The backgrounds we consider are Drell-Yan ($Z/\gamma \rightarrow ee, \mu\mu$), WZ , ZZ , $W\gamma$ and W + fake lepton, where the fake lepton is a jet which has been mistakenly identified as a lepton. These contributions are typically much smaller than our signal samples from the previous section, and in all our fits we fix these to their expected values.

Our fake background is data driven and estimated by first determining the probability for a jet or tracks to fake an electron or muon. We then apply these fake rates to our W + *jet* data samples, and apply all other analysis cuts to establish the contribution from this background. All other backgrounds are determined from Monte Carlo.

A summary of the numbers of “background” events expected after the requirement of 2 isolated leptons (and $\cancel{E}_T^{sig} < 2.5$ if ee or $\mu\mu$) is given in Table 4.

	$e\mu$	ee	$\mu\mu$	$\ell\ell$
$DY \rightarrow ee$	0	15.38 ± 3.2	0	15.4 ± 3.2
$DY \rightarrow \mu\mu$	9.3 ± 0.8	0	11.6 ± 2.4	20.8 ± 3.2
WZ	0.70 ± 0.06	1.26 ± 0.09	1.11 ± 0.08	3.07 ± 2.3
ZZ	0.07 ± 0.01	0.47 ± 0.03	0.42 ± 0.03	0.96 ± 0.07
$W\gamma$	1.2 ± 0.5	1.8 ± 0.7	0	3.0 ± 1.2
$W + j$	3.05 ± 0.32	2.12 ± 0.39	1.60 ± 0.15	6.8 ± 0.5

Table 4: Summary of expected background contributions. Uncertainties are statistical only, except for the W + fake lepton background, which includes the systematic uncertainty.

5 Data and grand summary of expectations

Table 5 shows the summary of all the signal and background expectations discussed in the previous sections. The average luminosity for the data sample used for this analysis is $184 \pm 11 \text{ pb}^{-1}$.

The integrated luminosities for ee , $e\mu$ and $\mu\mu$ are 363.2 ± 21.8 , 356.3 ± 21.4 , and $364.2 \pm 21.8 \text{ pb}^{-1}$ respectively. The differences for the various channels are due to different detector quality requirements. The errors on signal and backgrounds include both statistical and systematics uncertainties on acceptances. Also shown are the number of observed events in each channel from our data samples.

	$e\mu$	ee	$\mu\mu$	ll
“Signal” processes				
$t\bar{t}$	10.00 ± 0.7	3.61 ± 0.5	3.42 ± 0.4	17 ± 1.6
WW	13.8 ± 0.8	5.2 ± 0.4	4.3 ± 0.3	23.3 ± 1.5
$Z \rightarrow \tau\tau$	57.8 ± 4	1.1 ± 0.2	0.6 ± 0.1	59.5 ± 4.3
“Background” processes				
$DY \rightarrow ee$	0	15.38 ± 3.2	0	15.4 ± 3.2
$DY \rightarrow \mu\mu$	9.3 ± 0.8	0	11.6 ± 2.4	20.8 ± 3.2
WZ	0.70 ± 0.06	1.26 ± 0.09	1.11 ± 0.08	3.07 ± 2.3
ZZ	0.07 ± 0.01	0.47 ± 0.03	0.42 ± 0.03	0.96 ± 0.07
$W\gamma$	1.2 ± 0.5	1.8 ± 0.7	0	3.0 ± 1.2
$W + j$	3.05 ± 0.32	2.12 ± 0.39	1.60 ± 0.15	6.8 ± 0.5
Total expected “Signal + Background” event count				
	96 ± 4	31 ± 3	23 ± 2	150 ± 9
“CDF Data”				
Data	103	24	29	156

Table 5: Grand summary of expected and observed numbers of events in $\sim 360 \text{ pb}^{-1}$

6 The \cancel{E}_T - N_{jet} distributions for data and MC

Figures 1, 2 and 3 show the data and all the expected SM contributions discussed in the previous sections, in the \cancel{E}_T - N_{jet} phase space that we fit, for $e\mu$, ee and $\mu\mu$ respectively.

In the $e\mu$ channel, the $t\bar{t}$, WW and $Z \rightarrow \tau\tau$ distributions are normalized to unity (their total normalization is allowed to float in the fit). All the other distributions are lumped together and fixed to their expected values (and are normalized as such in the figures).

For the ee and $\mu\mu$ channels the same is true as for $e\mu$ **except** that because the \cancel{E}_T^{sig} is so effective in reducing DY (including $DY \rightarrow \tau\tau$), $Z \rightarrow \tau\tau$ in these channels is treated as one of the “other” backgrounds and fixed to its estimated value.

We see that our floating distributions ($t\bar{t}$, WW and $Z \rightarrow \tau\tau$) fall in distinctively different regions in this phase space which is what allows us to extract their cross sections so effectively. In the ee and $\mu\mu$ channels we see how the \cancel{E}_T^{sig} requirement has distorted the shape for the “other backgrounds”, a necessary consequence of removing most of the Drell-Yan.

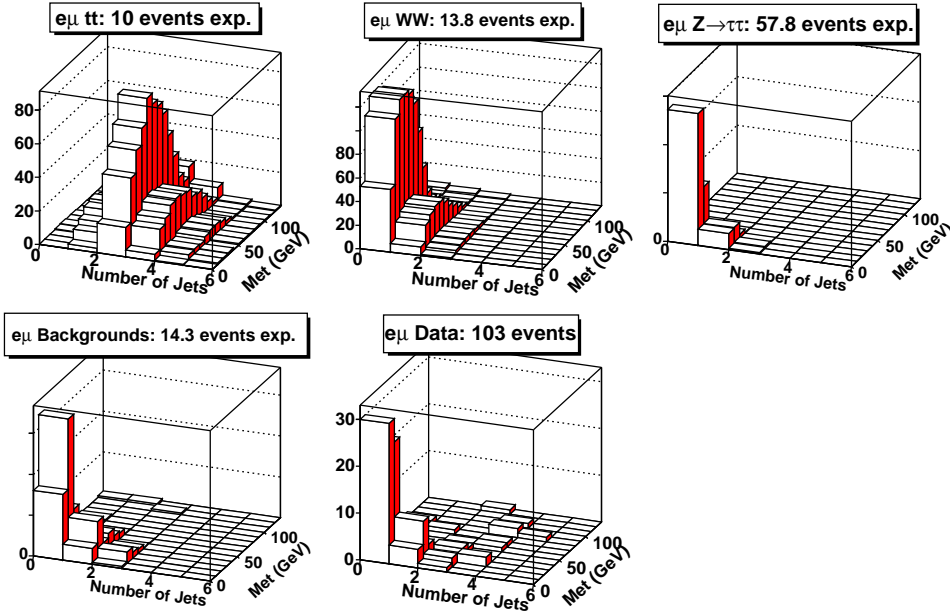


Figure 1: The $e\mu$ 2-D \cancel{E}_T - N_{jet} distributions for the SM “signal” sources, “background” sources (summed together) and from 360 pb^{-1} of data.

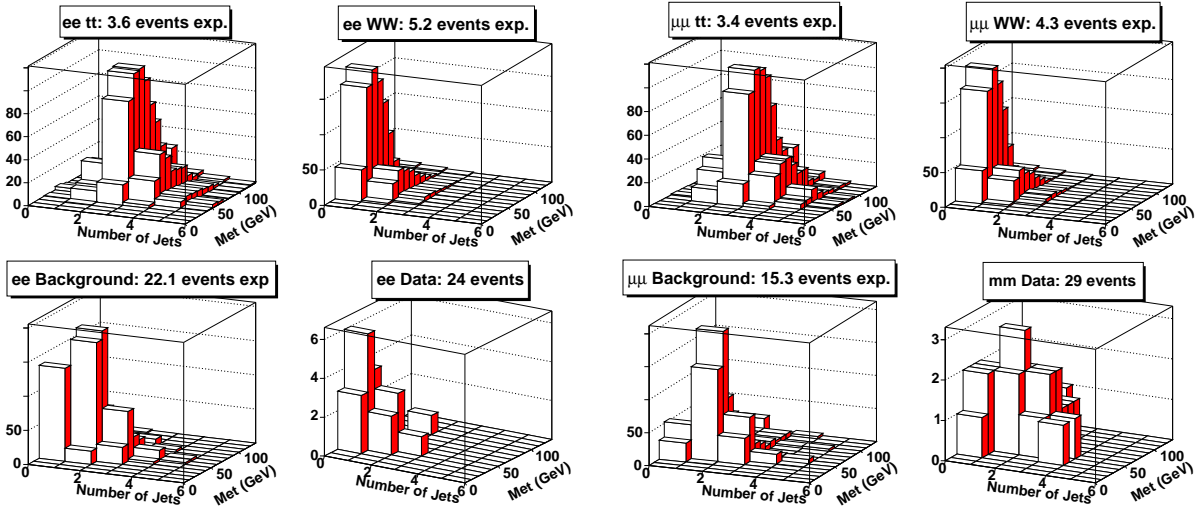


Figure 2: The ee 2-D \cancel{E}_T - N_{jet} distributions for the SM “signal” sources, “background” sources (summed together) and from 360 pb^{-1} of data.

Figure 3: The $\mu\mu$ 2-D \cancel{E}_T - N_{jet} distributions for the SM “signal” sources, “background” sources (summed together) and from 360 pb^{-1} of data.

7 The Likelihood fit technique

We form a Likelihood function from the Poisson probabilities comparing each bin in the \cancel{E}_T - N_{jet} space of the data with that of all the SM contributions. We minimize the negative of the logarithm of this Likelihood function using the CERN package MINUIT [3].

If we consider only the Standard Model contributions, the data distribution must be given by (in the $e\mu$ channel);

$$\frac{\partial^2 N}{\partial \cancel{E}_T \partial N_{jets}} = \alpha N_{t\bar{t}} + \beta N_{WW} + \gamma N_{Z \rightarrow \tau\tau} + n_{other} \quad (1)$$

Where the $t\bar{t}$, WW and $Z \rightarrow \tau\tau$ distributions (N_i) are normalized to 1, and the parameters α , β and γ are the fit number of events from each contribution, and are related to the respective cross-sections through

$$N = \sigma A \mathcal{L} \quad (2)$$

where σ is the cross section, A is total acceptance including the branching ratios, and \mathcal{L} is the integrated luminosity (properly weighted as discussed above).

The distributions of the ‘‘other’’ SM sources are normalized and fixed to the number of expected events, as given in Table 4.

We define the likelihood as:

$$L = \prod_i \rho_i \quad (3)$$

where i is over all bins in our 2-D distributions, and where:

$$\rho_i = \frac{\mu_i^{n_i} e^{-\mu_i}}{n_i!} \quad (4)$$

and n_i is the data distribution bin content for that particular bin and μ_i is the total expected number given by:

$$\mu_i = \alpha N_{t\bar{t}_i} + \beta N_{WW_i} + \gamma N_{Z \rightarrow \tau\tau_i} + n_{other_i} \quad (5)$$

We minimize $-\ln(L)$ as a function of α , β and γ to find the respective ‘‘best fit’’ contributions to the data sample.

The actual form of the likelihood function we use for our fit is more complicated than this because in our cross section measurements we have to account for systematic errors in all the acceptances, and the luminosity. We do this by adding Gaussian constraints for each acceptance and the luminosity. That is the likelihood function in equation (3) is multiplied by terms of the form:

$$G_f = e^{-\frac{(A_f - \hat{A}_f)^2}{2\sigma_{A_f}^2}} \quad (6)$$

where f refers to a given acceptance (or the luminosity) for each source, \hat{A}_f is its expected value, σ_{A_f} is its uncertainty, and A_f is its value in the fit that is allowed to float only insofar that G_f doesn't significantly reduce the Likelihood.

So in fact, in our fit α , β and γ are actually of the form:

$$\alpha_i = \sigma_i A_i \mathcal{L} \quad (7)$$

with the acceptances and luminosity now “free” (but Gaussian constrained) parameters in our fit. Therefore the errors returned by the fit on the cross sections include the effect of our acceptance and luminosity systematics.

Another important source of systematics is related to the shapes of our fitted MC distributions, which are added in quadrature after the fit is done and found from variations in the measured cross sections using Monte Carlo generated pseudo-experiments. We summarize the sources of shape systematics later.

We have performed extensive tests of this procedure with the use of pseudo-experiments.

8 $Z \rightarrow \tau\tau$ cross-section additional considerations.

One of our aims is to measure the $p\bar{p} \rightarrow Z \rightarrow \tau^+\tau^-$ cross section, where τ 's decay leptonically. However our Monte Carlo sample is for $Z/\gamma^* \rightarrow \tau^+\tau^-$, so we have remove the γ^* contribution. We want to estimate the cross section number for the true di-tau mass (at HEPG level) within the range $66 < M_{\tau\tau} < 116 \text{ GeV}/c^2$. Therefore, we define the acceptance, α , as the number of $Z/\gamma^* \rightarrow \tau\tau$ events in this mass window which pass our $e\mu$ channel selection criteria.

$$\alpha = \frac{N_{pass \text{ selection reqs}}[in]}{N_{generated}[in]} \quad (8)$$

where both numerator and denominator are restricted to events within the mass window. We use two Monte Carlo samples for estimating the acceptance. One is not big enough and has a very limited number of events passing our selection criteria, and the other has a lepton filter (requiring at least a generator level lepton with $P_T > 17$ in each event) cut and has enough events passing our selection criteria. We use the first one to calculate a correction factor to account for the cuts applied in the second sample.

We fit to the total number of events, N_{tot} , coming from $Z/\gamma^* \rightarrow \tau\tau$ and treat the contribution of events from outside the mass window as a correction factor, f^α .

$$f^\alpha = \frac{N_{pass \text{ selection}}[all]}{N_{pass, \text{election}}[in]} \quad (9)$$

To estimate f^α , we use Pythia Monte Carlo samples.

The cross-section expression becomes:

$$\sigma_{in} = \frac{N_{tot}}{f^\alpha} \frac{1}{2 \times BR(\tau \rightarrow e) \times BR(\tau \rightarrow \mu)} \frac{1}{\alpha \times \epsilon_{sc-factors, trig} \times L} \quad (10)$$

where the branching ratios are taken from the PDG. Ideally we should subtract the contribution from $\gamma^* \rightarrow \tau\tau$ and the interference between γ^* and Z^0 , to determine just the $Z^0 \rightarrow \tau\tau$ cross-section.

Based on the calculation done in other CDF analyses, this contribution is around 0.3% of the total, within the Z mass window, well below our total uncertainty on the cross section, so we do not correct for it.

9 Systematics

We have two classes of systematics that we treat differently in our analysis, one, the systematic uncertainty (from various sources) on the acceptances themselves, and a second due to the effect on the fitted cross-sections from changes in the \cancel{E}_T - N_{jet} template shapes due to various sources. The following 2 subsections give a brief overview of our two systematic sources.

9.1 Acceptance systematics

A summary of our acceptance systematics is given in Table 6. We incorporate these systematics in our fit by allowing the acceptances to vary in the likelihood function within a Gaussian constraint (of width given by the systematic error) as discussed in section 7. In addition, although not explicitly mentioned above, we have a similar Gaussian constraint for the luminosity (of width 6%).

Source	$t\bar{t}(ee)$	$t\bar{t}(e\mu)$	$t\bar{t}(\mu\mu)$	WW(ee)	WW($e\mu$)	WW($\mu\mu$)	$Z \rightarrow \tau\tau (e\mu)$
JES	5%	0	6%	1%	0	1%	0
ISR	+0 – 8%	+0 – 4%	+0 – 6%	5%	5%	5%	5%
FSR	+0 – 7%	+0 – 3%	+0 – 5%	na	na	na	na
PDF	(1%)	(1%)	(1%)	(1%)	(1%)	(1%)	(1%)
Multiple Int.	3%	3%	3%	0%	0%	0%	3%
Lepton SF	3%	3%	2%	4%	3%	2%	3%
Track Iso	2%	2%	2%	2%	2%	2%	2%
Metsig cut	3%	0	3%	3%	0	3%	0
total	+8 – 13%	+5 – 7%	+8 – 11%	7%	6%	7%	7%

Table 6: Summary of systematic uncertainties on the acceptance for each “signal” process. Note \cancel{E}_T^{sig} does not apply to $Z \rightarrow \tau\tau$ as we only fit for this in the $e\mu$ channel.

9.2 Shape systematics

We have investigated the effect of sources of uncertainties on the shapes of the \cancel{E}_T - N_{jet} distributions. These include jet energy scale, jet multiplicities (ISR/FSR), our modeling of \cancel{E}_T and \cancel{E}_T^{sig} , MC generator, and PDF’s. We use pseudo-experiments to calculate all our expected shape systematic errors, by observing the effect on the fitted cross sections as the shapes are varied according to a particular effect. These are all summarized in Table 7.

Source	tt $e\mu$	ww $e\mu$	$Z \rightarrow \tau\tau e\mu$	tt (full)	ww (full)
JES	-1 + 6%	-1 + 4%	-1 + 2%	-2 + 7%	-1 + 5%
ISR	-2 + 4%	$\pm 1\%$	$\pm 1\%$	-2 + 5%	$\pm 1\%$
FSR	$\pm 1\%$	—	—	—	—
Total	-2 + 7%	-1 + 4%	-1 + 2%	-3 + 8%	-1 + 5%

Table 7: The shape systematic errors summary on the $e\mu$ and full fit.

10 Fit results

We fit the data to our SM signal templates using various scenarios which are all summarized in Table 8. The first error given includes statistical and systematic on the acceptances and luminosity, while the second error is that from shape variations.

In Table 8 we show our cross section measurements for two cases: one where all the signal processes are allowed to float simultaneously, and the other where only the measured process is allowed to float while the others are fixed to their expected values within Gaussian constraints on their errors. The values from this latter case are more precise, so we consider them as the measured cross sections for a given process, and these are summarized in Table 9, and compared to theoretical expectations.

Process	$e\mu$	$ee + \mu\mu + e\mu$	theoretical
$\sigma(t\bar{t})$ (WW, $Z \rightarrow \tau\tau$ fixed)	$9.3^{+3.1}_{-2.6}(fit)^{+0.7}_{-0.2}(shape)$ pb	$8.4^{+2.5}_{-2.1}(fit)^{+0.7}_{-0.3}(shape)$ pb	6.7 ± 0.3 pb
$\sigma(t\bar{t})$ (all floating)	$9.3^{+3.1}_{-2.6}(fit)^{+0.7}_{-0.2}(shape)$ pb	$8.5^{+2.6}_{-2.2}(fit)^{+0.7}_{-0.3}(shape)$ pb	-
$\sigma(WW)$ ($t\bar{t}$, $Z \rightarrow \tau\tau$ fixed)	$12.3^{+5.3}_{-4.4}(fit)^{+0.5}_{-0.1}(shape)$ pb	$16.1^{+5.0}_{-4.3}(fit)^{+0.8}_{-0.2}(shape)$ pb	12.5 ± 0.8 pb
$\sigma(WW)$ (all floating)	$11.4^{+5.2}_{-4.3}(fit)^{+0.5}_{-0.1}(shape)$ pb	$16.3^{+5.1}_{-4.4}(fit)^{+0.8}_{-0.2}(shape)$ pb	-
$\sigma(Z \rightarrow \tau\tau)$ ($t\bar{t}$, WW fixed)	$292.7^{+48.9}_{-45.1}(fit)^{+5.9}_{-2.9}(shape)$ pb	-	253.1 ± 0.5 pb
$\sigma(Z \rightarrow \tau\tau)$ (all floating)	$291.4^{+49.5}_{-46.0}(fit)^{+5.8}_{-2.9}(shape)$ pb	-	-

Table 8: Cross-section measurements from various data fit scenarios, for $360 pb^{-1}$ of data. For each channel, we extract two sets of values: either all the cross-sections are left unconstrained, or two are fixed to the SM expectation. By *stat* we mean the error returned by the fit, which includes the statistical error, the systematics error on acceptance and luminosity; *shape* refers to the shape systematics in this case (see section 9.2). The final results for the SM cross-sections measured with $360 pb^{-1}$ are shown.

Process	Measured cross-section (pb)
$\sigma(t\bar{t})$	$8.4^{+2.5}_{-2.1}(fit)^{+0.7}_{-0.3}(shape)$
$\sigma(WW)$	$16.1^{+5.0}_{-4.3}(fit)^{+0.8}_{-0.2}(shape)$
$\sigma(Z \rightarrow \tau\tau)$	$292.7^{+48.9}_{-45.1}(fit)^{+5.9}_{-2.9}(shape)$

Table 9: Cross-section results for $360 pb^{-1}$ of CDF II data.

In Figures 4, 5 and 6 we show the $1-\sigma$ confidence level contour plots for our $e\mu$ fit. In these plots we include statistical errors, acceptance systematic errors and luminosity systematic errors,

the shape systematic errors are not included in these plots and can be simply added in quadrature. Also these figures represent confidence limit projections when all signal processes are allowed to float in our fit simultaneously. In figure 7 we see the same kind of plot but for the fit performed in the $ee + \mu\mu + e\mu$ channels for the WW and $t\bar{t}$ cross sections.

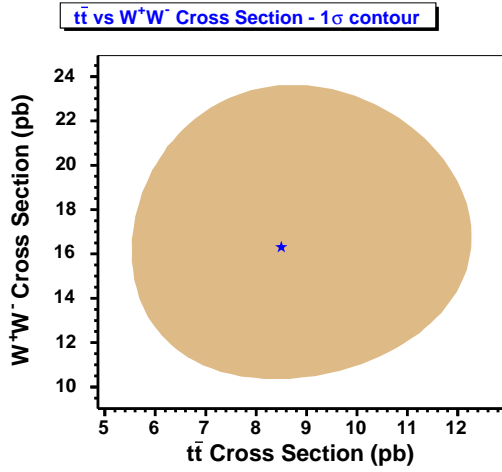


Figure 4: 1-sigma confidence level plot, in terms of the fitted cross-sections, σ_{WW} vs $\sigma_{t\bar{t}}$, in $e\mu$ channel. Shape systematics are not included.

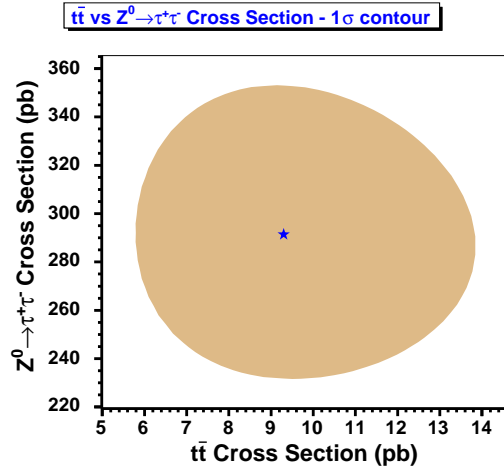


Figure 5: 1-sigma confidence level plot, in terms of the fitted cross-sections, $\sigma_{Z \rightarrow \tau\tau}$ vs $\sigma_{t\bar{t}}$, in $e\mu$ channel. Shape systematics are not included.

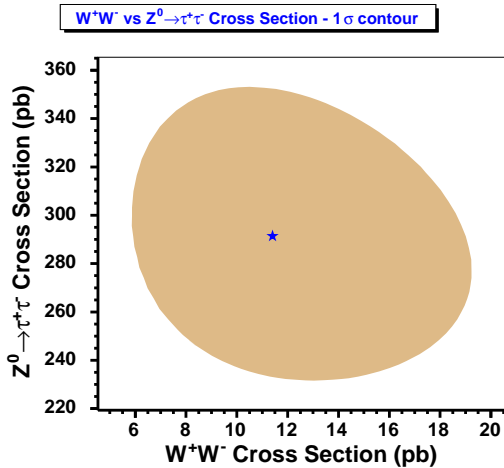


Figure 6: 1-sigma confidence level plot, in terms of the fitted cross-sections, $\sigma_{Z \rightarrow \tau\tau}$ vs $\sigma_{W^+W^-}$, in $e-\mu$ channel. Shape systematics are not included.

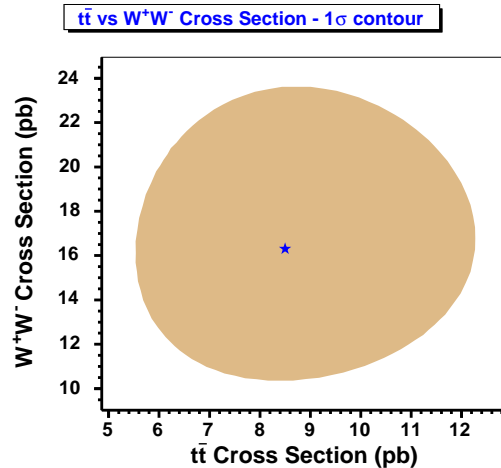


Figure 7: 1-sigma confidence level plot, in terms of the fitted cross-sections, $\sigma_{W^+W^-}$ vs $\sigma_{t\bar{t}}$, in $e-e+\mu\mu$ channel. Shape systematics are not included.

11 Conclusions

We have developed and given our first results for a potentially powerful method for extracting SM cross sections in the high- P_T dilepton sample with optimal statistical power while maintaining high signal purity. Our results are summarized in Tables 8 and 9.

This method might also be very useful for new physics searches, which is one of our goals in its application, and we are currently exploring this potential.

12 Acknowledgments

We thank the Fermilab staff and the technical staffs of the participating institutions for their vital contributions. This work was supported by the U.S. Department of Energy and National Science Foundation; the Italian Istituto Nazionale di Fisica Nucleare; the Ministry of Education, Culture, Sports, Science and Technology of Japan; the Natural Sciences and Engineering Research Council of Canada; the National Science Council of the Republic of China; the Swiss National Science Foundation; the A.P. Sloan Foundation; the Bundesministerium fuer Bildung und Forschung, Germany; the Korean Science and Engineering Foundation and the Korean Research Foundation; the Particle Physics and Astronomy Research Council and the Royal Society, UK; the Russian Foundation for Basic Research; the Comision Interministerial de Ciencia y Tecnologia, Spain; and in part by the European Community's Human Potential Programme under contract HPRN-CT-20002, Probe for New Physics.

References

- [1] F. Abe, et al., The CDF Collaboration, Phys. Rev. Lett. 80, 2779 (1998)
- [2] J.M. Campbell, R.K. Ellis, An update on vector boson pair production at hadron colliders, hep-ph/9905386
- [3] F. James, Minit Reference Manual, Version 94.1
<http://wwwasdoc.web.cern.ch/wwwasdoc/WWW/minuit/minmain/minmain.html>.